



# Fluorometric and colorimetric quantitative analysis platform for acid phosphatase by cerium ions-directed AIE and oxidase-like activity

Qing Li<sup>1,2</sup> · Yue Gao<sup>1</sup> · Si-Hua Liu<sup>1</sup>

Received: 17 October 2023 / Revised: 20 November 2023 / Accepted: 8 December 2023 / Published online: 27 December 2023  
© The Author(s), under exclusive licence to Springer-Verlag GmbH, DE part of Springer Nature 2023

## Abstract

A facile and sensitive fluorescent and colorimetric dual-readout assay for detection of acid phosphatase (ACP) was developed via Ce(III) ions-directed aggregation-induced emission (AIE) of glutathione-protected gold nanoclusters (GSH-AuNCs) and oxidase-mimicking activity of Ce(IV) ions. Free Ce(IV) ions exhibited a strong oxidase-mimetic activity, catalytically oxidizing colorless 3,3',5,5'-tetramethylbenzidine (TMB) into its blue product oxTMB in the presence of dissolved O<sub>2</sub>, thus triggering a remarkable color reaction detected visually. ACP can hydrolyze L-ascorbic acid-2-phosphate (AAP) with the production of ascorbic acid (AA). The AA is able to reduce Ce(IV) ions to Ce(III) ions, thus quenching the oxidase-mimetic activity of Ce(IV) ions. Meanwhile, Ce(III) ions induce AIE of GSH-AuNCs, resulting in the enhancement of the fluorescence signal of GSH-AuNCs. Both the fluorescent and colorimetric dual-mode analysis platforms exhibit a sensitive response to ACP, providing detection limits as low as 0.101 U/L and 0.200 U/L, respectively. Besides, this fabricated dual-mode detection platform holds the potential for analysis of ACP in human serum samples and screening inhibitors for ACP. With good performance and practicability, this study shows promising application in the convenient and reliable determination of ACP activity.

**Keywords** GSH-AuNCs · Fluorescence sensor · Colorimetric analysis · Dual-mode · Acid phosphatase · Aggregation-induced emission

## Introduction

Acid phosphatase (ACP) is a versatile enzyme found widely in the fluids and tissues of mammals, which hydrolyzes the ester—phosphate bonds of organophosphorus compounds in weak acid environment [1]. As a phosphomonoesters, ACP plays an essential role in modulating a range of intracellular biological alterations [2, 3]. The atypical levels of ACP suggest the progression of diseases such as disseminated prostate cancer, Gaucher's syndrome, Paget's syndrome, and specific ailments associated with kidneys and bones [4, 5].

Therefore, ACP is regarded as a crucial biomarker and predictive indicator. Furthermore, certain variations of ACPs, such as phosphatidic acid phosphatase type 2C and tartrate-resistant acid phosphatase, have been identified as potential targets for medication [6]. Therefore, the development of sensitive and selective ACP detection method is of great significance for the diagnosis and drug screening.

To date, several strategies have been developed for detection of ACP, such as high-performance liquid chromatography [7], electrochemical methods [8], radioimmunoassay [9], etc. Despite some outstanding achievements in research laboratories, these methods often require complex instrumentation, cumbersome operation [10]. Taking these drawbacks into full consideration, great efforts have been made to develop convenient and sensitive method for ACP determination. In virtue of straightforward signal output and outcome visualization, optical ACP sensors have gained wide attention in recent years [11–15]. However, most ACP assays relied on target-induced single-signal response changes, where light source fluctuations or environmental influences can lead to false positive results that directly affect the accuracy and reliability of the developed methods, which can

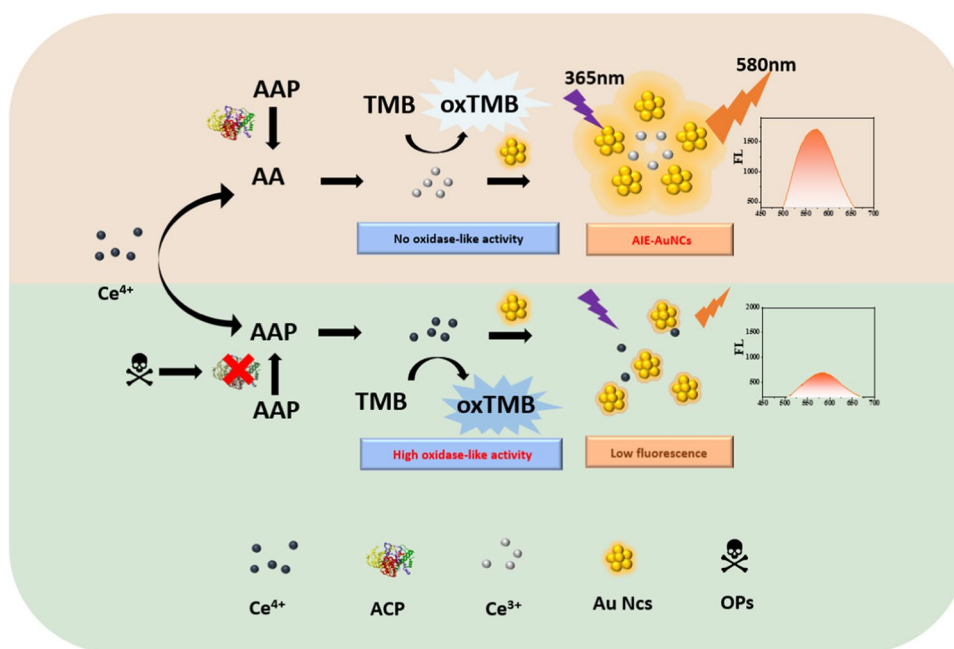
✉ Qing Li  
qingli@hut.edu.cn

✉ Si-Hua Liu  
sihua0526@hut.edu.cn

<sup>1</sup> College of Life Science and Chemistry, Hunan University of Technology, Zhuzhou 412007, China

<sup>2</sup> State Key Laboratory of Chemo/Bio-Sensing and Chemometrics, College of Chemistry and Chemical Engineering, Hunan University, Changsha 410082, People's Republic of China

**Scheme 1** Schematic depiction of the design of the dual-mode fluorescence-colorimetric strategy for ACP detection and its inhibitor screening



be limited in practical applications [16, 17]. In comparison to single-signal ACP assay, multi-mode detection improves accuracy of results and is expected to provide more reliable results because it can offer different kinds of output signals for self-validation and self-correction, thus greatly reducing false and incorrect results. Therefore, it is particularly significant to construct a facile and robust strategy to implement multi-mode efficient for ACP determination.

Ionic enzyme-mimetics have not only high catalytic activity compared with biological enzymes, but also stable and economical characteristics of simulated enzymes, which have received increasing attention [18–20]. Several ions such as  $\text{Cu}^{2+}$  and  $\text{Ce}^{4+}$  have also been demonstrated to possess enzyme-mimicking activity [21, 22]. In comparison with biological enzymes and nanozymes, ionic enzyme-mimetics offer the merits of facilitating substrate access to active sites, simplifying the catalytic system by eliminating the need for complex structural manipulation, and providing readily available alternatives to laborious processes. These advantages contribute to the favorable characteristics of ionic enzyme-mimetic catalyzed colorimetric method, including quick response, facile and low cost.

The exceptional fluorescence properties, convenient preparation and dispersion stability of Au nanoclusters (AuNCs) have made gained significant attention in various fields, including chemical and biological sensing, drug delivery and bioimaging [23–26]. The fluorescence intensity of AuNCs can be further enhanced through the AIE effect, which is based on the limitation of intramolecular movements that activate non-radiative transition pathways [27]. Metal ions, including  $\text{Al}^{3+}$ ,  $\text{Zn}^{2+}$ ,  $\text{Cd}^{2+}$ ,  $\text{Gd}^{3+}$ ,  $\text{Pb}^{2+}$  and  $\text{Ce}^{3+}$ , have been found to induce aggregation of AuNCs in dilute solutions,

leading to stronger fluorescence quantum yield by the AIE effect [28–31]. Therefore, the AIE effect provides a new strategy for regulating the “on–off” switching of fluorescence signals in AuNCs.

Herein, a strategy for dual-mode sensing of ACP activity is proposed by combining the oxidase-mimetic catalytic feature of  $\text{Ce}^{4+}$  ions with aggregation-induced emission of GSH-AuNCs by  $\text{Ce}^{3+}$  ions. As displayed in Scheme 1, the process begins with L-ascorbic acid 2-phosphate (AAP), which is a derivative of ascorbic acid (AA) that undergoes esterification of the hydroxyl group. In the presence of ACP, AAP is hydrolyzed to generate reductive AA. This AA then reduces  $\text{Ce}^{4+}$  ions to  $\text{Ce}^{3+}$  ions. The free  $\text{Ce}^{4+}$  ions possess oxidase-mimetic activity and catalyze TMB chromogenic reaction. However, the  $\text{Ce}^{3+}$  ions formed from the reduction of  $\text{Ce}^{4+}$  ions exhibit significantly decreased oxidase-like activity, leading an obvious suppression of the catalytic TMB oxidation. Additionally, the  $\text{Ce}^{3+}$  ions form complexes with the carboxyl-group of glutathione on the exterior of GSH-AuNCs through electrostatic aggregation. This complexation limits nonradiative relaxation of the excited states by restricting the intramolecular rotation-vibrational motion, resulting in an enhancement of the fluorescence signal of GSH-AuNCs through AIE effect. The appearance of organophosphorus pesticide (OPs) can irreversibly inhibit ACP activity and block the production of AA, preventing the conversion of  $\text{Ce}^{4+}$  ions to  $\text{Ce}^{3+}$  ions. Consequently, the catalytic TMB oxidation was recovered, whereas the AIE of GSH-AuNCs obtained from  $\text{Ce}^{3+}$  ions suppressed. The valence state of  $\text{Ce}^{4+}$  ions can be changed through the activity of ACP, thereby obtaining a “turn off” colorimetric signal and “turn on” fluorescence signal. With only  $\text{Ce(IV)}$  ions as

the intermediary, GSH-AuNCs and TMB serve as the two different signals conversion elements, the enhancement of fluorescence and the reduction of the colorimetric signal during ACP sensing are independent and can be self-validation, simplifying the construction through this straightforward method. Therefore, this dual-mode response strategy has great potential in detecting ACP activity in biological samples and screening potential ACP inhibitors.

## Experimental section

### Reagents and instruments

Glutathione (reduced form),  $\text{HAuCl}_4 \cdot 4\text{H}_2\text{O}$ ,  $(\text{NH}_4)_4\text{Ce}(\text{SO}_4)_4$  and  $\text{Ce}_2(\text{SO}_4)_3$  were acquired from Macklin Biochemical Co., Ltd. (Shanghai, China). L-ascorbic acid 2-phosphate trisodium salt (AAP), acid phosphatase was ordered from Yuanye Bio-Technology Co., Ltd (China). Malathion and chlorpyrifos was gained from Gbw (China). Serum samples were obtained from anonymous donors at Zhuzhou Central Hospital, China.

The fluorescence measurements were performed at room temperature on F-7100 fluorescence spectrometer (Hitachi Ltd., Tokyo, Japan). The fluorescence spectrums of GSH-AuNCs were recorded from 385 to 700 nm with an excitation wavelength at 365 nm. Ultraviolet–visible absorption spectrum was carried out on Lambda 750 s UV–vis spectrometer (PerkinElmer, USA).

### Synthesis of GSH-AuNCs

GSH-AuNCs were synthesized based on previously reported literature [27]. 1 mL  $\text{HAuCl}_4 \cdot 4\text{H}_2\text{O}$  (20 mM) solutions and 0.3 mL GSH (100 mM) were added into 8.7 mL deionized water and incubated at room temperature for 5 min. The incubation temperature was increased by 70 °C, then the mixture solution was gently stirred for 24 h. Finally, the light-yellow product was obtained and placed in the fridge at 4 °C before use.

### Fluorescent and colorimetric determination of ACP

For fluorescence assay, different concentrations of ACP solution (5  $\mu\text{L}$ , 0–13 U/L) and 10  $\mu\text{L}$  AAP solution (0.25 mM) were introduced into the mixture of 10  $\mu\text{L}$   $\text{Ce}^{4+}$  solution (40  $\mu\text{M}$ ), 5  $\mu\text{L}$  GSH-AuNCs solution and 70  $\mu\text{L}$  HEPES buffer (pH 5.0, 10 mM), and incubated at room temperature for 30 min. After that, the mixture solutions were recorded on the fluorescence spectrophotometer under the excitation wavelength of 365 nm.

For colorimetric analysis, the reaction of ACP enzyme catalyzed substrate is the same as above. After that, 10  $\mu\text{L}$

of 5 mM TMB solution (dissolved in ethanol) was incubated with the above mixture and reacted for 10 min. Then, the reaction solutions were measured by the UV–vis spectrophotometer.

### Analysis of ACP in real samples

100  $\mu\text{L}$  of sera samples were centrifuged at 10,000 rpm for 10 min, the resulting supernatant was diluted to 1 mL with HEPES buffer (pH 5.0, 10 mM). The obtained 10% diluted serum samples were added into different standard concentration of ACP to acquire spiked samples and determined under the same procedure as above.

### Investigation of potential for screening of ACP inhibitors

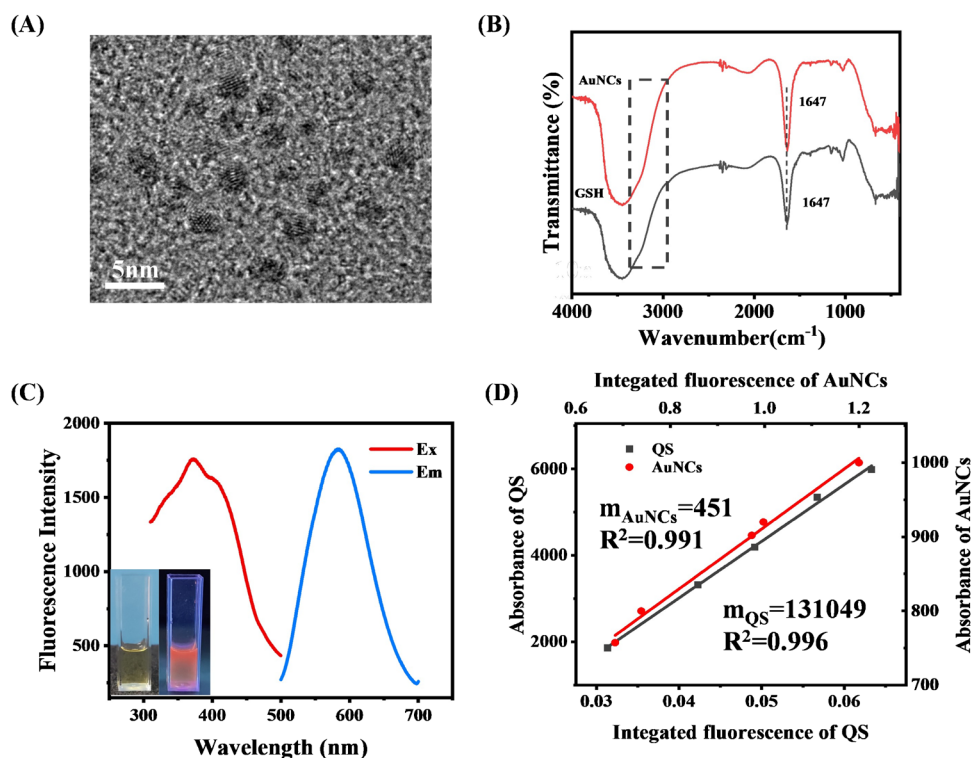
Different concentrations of OPs were added to 70  $\mu\text{L}$  mixture containing 13 U/L ACP and 10 mM HEPES buffer (pH 5.0). The resultant solutions were reacted under 37 °C for 15 min. The following experimental procedures were the same as those for ACP activity assay. The inhibition efficiency (IE) was analyzed by the following equation:  $\text{IE}\% = (\text{F}_{\text{inhibitor}} - \text{F}_{\text{no inhibitor}}) / (\text{F}_0 - \text{F}_{\text{no inhibitor}}) \times 100\%$ ,  $\text{IE}\% = (\text{A}_{\text{inhibitor}} - \text{A}_{\text{no inhibitor}}) / (\text{A}_0 - \text{A}_{\text{no inhibitor}}) \times 100\%$ , where  $\text{F}_{\text{inhibitor}}/\text{A}_{\text{inhibitor}}$  and  $\text{F}_{\text{no inhibitor}}/\text{A}_{\text{no inhibitor}}$  represent the signal intensity of reaction system with and without OPs, respectively.  $\text{F}_0/\text{A}_0$  refers to the signal intensity of reaction system without ACP and OPs.

## Results and discussion

### Preparation and characterization of GSH-AuNCs

GSH was used as reductant and stabilizing agent for preparation of fluorescent GSH-AuNCs. The surface morphology of synthesized GSH-AuNCs was characterized by transmission electron microscopy (TEM). According to the TEM image showed in Fig. 1A, the GSH-AuNCs displayed mono-dispersed with an average diameter of about 2 nm. Furthermore, we measured the dynamic light scattering (DLS) of GSH-AuNCs and found that the mean hydrodynamic diameter of GSH-AuNCs was approximately 2 nm (Figure S1). The evidence for successful encapsulating GSH with AuNCs was identified by Fourier-transform infrared spectroscopy (FTIR) analysis. As displayed by Fig. 1B, the characteristic peak at 1647  $\text{cm}^{-1}$  was corresponding to stretching vibration of for  $\text{COO}^-$ , and the appearance of band located at 3352–2959  $\text{cm}^{-1}$  was attributed to bending and stretching vibration of O–H, respectively. The UV–vis absorption spectra of GSH-AuNCs were also investigated, as shown in Figure S2. In comparison with GSH alone, the prepared GSH-AuNCs

**Fig. 1** (A) TEM image. (B) FTIR spectra of GSH and GSH-AuNCs. (C) The maximum fluorescence excitation (red line) and emission (blue line) spectrum of GSH-AuNCs. (D) Representative analysis of quantum yield via comparison of GSH-AuNCs luminescent intensity vs. absorbance with that of quinine sulfate



presented a distinct absorption within the wavelength range of 300–400 nm. These results indicated that the GSH-AuNCs was successfully synthesized.

The maximum luminescence emission and excitation peak of the prepared GSH-AuNCs located at 580 nm and 365 nm, demonstrating a substantial Stokes shift of 215 nm (Fig. 1C). By using quinine sulfate as the reference, the GSH-AuNCs fluorescence quantum yield (QY) was calculated to be 0.3% (Fig. 1D). As revealed in Figure S3, the fluorescence emission of GSH-AuNCs is not affected in the pH range of 3–11, indicating that fluorescent GSH-AuNCs have a wide range of pH tolerance. Notably, the GSH-AuNCs also showed excellent salt tolerance, as shown in Figure S4. The fluorescence intensity of GSH-AuNCs did not change significantly when the concentration of NaCl was in the range of 0–100 mM. Furthermore, the GSH-AuNCs can maintain stable fluorescence intensity at 4°C for more than 4 weeks (Fig. S5). These results revealed that the prepared GSH-AuNCs exhibit a prominent chemical stability and photostability and hold potential application in practical environment analysis.

### AIE of GSH-AuNCs by Ce<sup>3+</sup> ions

The as-prepared GSH-AuNCs was then incubated with Ce<sup>3+</sup>, and the fluorescence properties of GSH-AuNCs-Ce<sup>3+</sup> was systematically investigated. Figure S6 showed that the fluorescence intensity of GSH-AuNCs was weak

when dispersed in aqueous solution. Interestingly, when Ce<sup>3+</sup> were added to the solution, an enhancement of fluorescence signal at 575 nm was observed. However, when Ce<sup>4+</sup> was incubated with GSH-AuNCs, the system can merely display noticeable fluorescence change. Accompanied by increasing the amount of Ce<sup>3+</sup>, the fluorescence emission of GSH-AuNCs is blue shifted to 575 nm and enhanced up to nearly 4-times when the concentration of Ce<sup>3+</sup> is 30 μM (Figure S7). As the main alteration of AIE originated from the ligand molecules, the Zeta potential changes of GSH-AuNCs before and after adding Ce<sup>3+</sup> were then monitored. Figure S8 showed that the zeta potential of GSH-AuNCs increased from -23.4 mV to -2.54 mV upon the addition of Ce<sup>3+</sup>, which suggested that there is electrostatic interaction between Ce<sup>3+</sup> and GSH-AuNCs. Significant aggregation of GSH-AuNCs triggered by Ce<sup>3+</sup> was observed from TEM images in Figure S9, large cluster are assembled from dispersive GSH-AuNCs. The dynamic light scattering (DLS) characterization (Figure S10) further confirmed the aggregation of GSH-AuNCs. The results from DLS revealed that the average size of the GSH-AuNCs-Ce<sup>3+</sup> system was noticeably larger compared to that of GSH-AuNCs. A correlation was found between the concentration of Ce<sup>3+</sup> and the size of agglomeration. As shown in Figure S11, as the concentration of Ce<sup>3+</sup> increased from 10 μM to 50 μM, the absorption peak of the GSH-AuNCs underwent a red shift and the absorption intensity gradually increased, indicating that the size of

GSH-AuNCs agglomeration increased with the increase of  $Ce^{3+}$  concentration.

Besides, FTIR spectrum were performed to study the interaction between  $Ce^{3+}$  and GSH-AuNCs. Compared with GSH-AuNCs, an evident distinction was observed in Figure S12, where the intensity of the characteristic stretching vibration of the carboxylate group at  $1647^{-1}$  and  $3315-2929\text{ cm}^{-1}$  in the GSH-AuNCs- $Ce^{3+}$  system was comparatively weaker than that of GSH-AuNCs. These results indicated that the  $Ce^{3+}$ -induced AuNCs aggregation was ascribed to the chelation of  $Ce^{3+}$  with carboxylate group on the exterior of GSH-AuNCs. Because of AIE mediated self-assemblies, the intramolecular vibration of the ligand is limited, the ligand-dependent non-radiative relaxation is inhibited, thus the fluorescence emission intensity of GSH-AuNCs is enhanced.

### Investigation of the oxidase-like activity of $Ce^{4+}$ ions

To explore the oxidase-like activity of  $Ce^{4+}$ , the chromogenic reaction of TMB was firstly studied. As shown in Figure S13, in the absence of  $Ce^{4+}$ , there is no absorption peak at 652 nm when the system contains TMB alone. However, it is showed a remarkable UV absorption peak at 652 nm when  $Ce^{4+}$  ions solution incubated with TMB. Comparatively,  $Ce^{3+}$  ions exhibit no apparent catalytic oxidation effect on TMB. This color change is due to the production of blue oxTMB, which means that  $Ce^{4+}$  can trigger the oxidation of TMB. To further demonstrate that  $Ce^{4+}$  ions can act as an oxidase-mimic but not as an oxidant to trigger TMB chromogenic reaction, the reactions of  $Ce^{4+}$  and TMB in saturated air and  $N_2$  atmosphere were explored. As depicted in Figure S14, TMB chromogenic reaction in the air-saturated atmosphere displayed an obvious color change, while that in  $N_2$  atmosphere is evidently impaired. This comparison suggested that chromogenic reaction indeed dependent on the presence of  $O_2$ , validating that  $Ce^{4+}$  can serve as an ionic oxidase-mimics and catalyze the redox reaction of dissolved  $O_2$  and TMB. The chromogenic reaction was also demonstrated by other substrate through the catalytic capacity of  $Ce^{4+}$  ions. As evident by Figure S15, in addition to the positively charged TMB substrate, two other chromogenic substrates, the negatively charged 2,2'-azinobis(3-ethylbenzothiazoline)-6-sulfonic acid (ABTS) and the neutral o-phenylenediamine (OPD), also exhibited notable color reactions when catalyzed by  $Ce^{4+}$ . These above results can further confirm that oxidase-like activity of  $Ce^{4+}$ , which can catalyze oxidation of substrate chromogenic reaction.

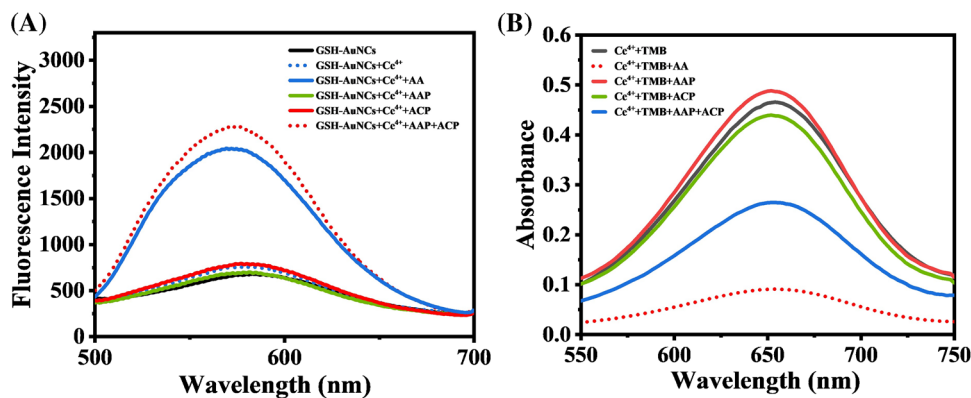
In order to further evaluate the catalytic ability of  $Ce^{4+}$  oxidase, the steady-state kinetic parameters of TMB were measured. Figure S16 present the typical Michaelis–Menten curve. Accordingly, the Michaelis–Menten constant ( $K_m$ ) for TMB catalysis by  $Ce^{4+}$  was determined to be 0.046 mM,

with a maximum velocity ( $V_{max}$ ) of  $1.006 \times 10^{-6}$  M/s. As shown in Table S1, this result suggested that  $Ce^{4+}$  exhibit comparable catalytic capability and efficiency in comparison to these nanozymes when it comes to oxidizing substrates, indicating  $Ce^{4+}$  ion can be adopted as a promising oxidase mimetic for appealing application.

### Feasibility evaluation of dual-mode fluorescent-colorimetric sensing platform for ACP

Encouraged by the key role of Ce ions-directed aggregation induced emission effect and oxidase-like activity, we further explore the usefulness of Ce ions in the field of biosensor, and try to fabricate dual-mode fluorescent-colorimetric detection platform for ACP activity analysis. Based on the aforementioned investigations,  $Ce^{3+}$  ions induce AIE effect of AuNCs and  $Ce^{4+}$  ions triggered oxidation of TMB, the valence state of Ce can be regulated by redox reaction to achieve the changes of fluorescence and colorimetric signal. It is well known that ACP can specifically catalyze AAP hydrolysis and yield free AA products. Considering that AA has reducing ability to  $Ce^{4+}$ , to proof this concept, the strategy envisioned above was subsequently applied to combine with the enzymatic reaction of ACP to direct the valence state of Ce and construct fluorescent and colorimetric dual-mode sensing strategy for ACP activity quantification. The fluorescence and UV–vis spectra of different reaction system were measured to survey the feasibility of the proposed sensing strategy. As presented in Fig. 2A, compared with  $Ce^{4+}$ -GSH-AuNCs system, when the  $Ce^{4+}$ -GSH-AuNCs system was introduced AAP or ACP, respectively, the fluorescence intensity of the system displayed a negligible change. However, there is an obvious fluorescence enhancement when the  $Ce^{4+}$ -GSH-AuNCs system incubated with AA. Remarkably, along with the addition with both AAP and ACP into  $Ce^{4+}$ -GSH-AuNCs system, an enhanced fluorescence signal was obtained. As exhibited in Fig. 2B, as anticipated, incubation of AA with  $Ce^{4+}$ -TMB system, the absorption peak at 652 nm was disappeared and the TMB colorimetric reaction was inhibited since the  $Ce^{4+}$  underwent a transformation into  $Ce^{3+}$  and consequently lost its capability to oxidize. While the addition of AAP and ACP with  $Ce^{4+}$  separately, TMB could be still catalytic oxidized by  $Ce^{4+}$  to produce oxTMB with an apparent absorption peak at 652 nm. when AAP and ACP coexisted in the  $Ce^{4+}$ -TMB system, absorbance at 652 nm decreased significantly. Based on these findings, it is suggested that, in the presence of ACP, the AAP substrate underwent hydrolysis to generate AA, which exhibit a specific ability to reduce  $Ce^{4+}$  ions to  $Ce^{3+}$  ions, thus “turn on” the AIE of AuNCs and “turn off” the oxidase-mimicking activity. Rely on the “bridge” substance of AA, the changes in fluorescence and colorimetric signals triggered by Ce ions can serve as indirect indicators

**Fig. 2** Feasibility for the fluorescent (A) and colorimetric (B) determination of ACP based on Ce ions-directed dual-mode detection strategy. Reactions were performed with 0.25 mM AAP, 10 U/L ACP at room temperature for 30 min. 40  $\mu$ M  $Ce^{4+}$ , 5 mM TMB and 50  $\mu$ M AA, 5  $\mu$ L GSH-AuNCs solution were used for all experiments



of ACP enzyme activity. Therefore, these results demonstrated that our suggested Ce ions-directed dual-mode detection strategy can be employed for ACP activity sensing.

### Optimization of reaction conditions

In order to acquire the best analytical performance, reaction condition including the pH value, the concentration of substrate AAP, ACP enzyme catalytic reaction time,  $Ce^{4+}$  concentration, TMB concentration and colorimetric reaction time was optimized. The activity of ACP enzyme is highly dependent on pH of buffer. Clearly, the enzyme is active in acidic environment, and the response performance of the enzyme with different pH in HEPES buffer is investigated. As shown in Figure S17, both response performance of fluorescence and colorimetric assay was best when the pH environment was at 5.0. Thereby, the optimal pH for ACP enzyme reaction was selected as 5.0. The concentration of substrate AAP was also an important factor for ACP enzymatic reaction since it is the source of AA, which affect the subsequent redox reaction. As shown in Figure S18, fluorescence signal-to-background ratio reached its maximum value at 0.25 mM, suggesting that the concentration of substrate AAP can be fixed at 0.25 mM for the following experiments. The time for ACP catalysis reaction was also surveyed, evident by Figure S19, the optimal ACP enzyme incubation time can be set at 30 min. Considering the key role of  $Ce^{4+}$ , the concentration of  $Ce^{4+}$  was also optimized. As illustrated in Figure S20, the fluorescence analytical performance kept the highest when the concentration of  $Ce^{4+}$  was 40  $\mu$ M. Under the above optimized reaction condition, TMB concentration and the discoloration reaction time was also investigated, as shown in Figure S21, the absorption intensity reached its maximum value at 5 mM of TMB. In Figure S22, the absorbance intensity became stronger along with the increased discoloration reaction time and reached to a plateau at 10 min. Therefore, the optimal colorimetric reaction condition is that the TMB concentration is 5 mM

and the reaction time is 10 min, and used for follow-up experiments.

### Fluorescent and colorimetric assay of acid phosphatase activity

The quantitative analysis of ACP activity was carried out by using fluorescent and colorimetric dual-mode strategy under the optimal experimental conditions. As present in Fig. 3A, the fluorescence intensity of reaction system is increased progressively with the increasing of ACP concentration from 0 U/L to 13 U/L, offering a “turn on” fluorescence signal for ACP activity analysis. Figure 3B displayed the plot of fluorescence intensity enhancement  $\Delta F = F - F_0$  ( $F_0$  and  $F$  are the fluorescence intensity of the system at 575 nm without and with ACP, respectively) against the concentration of ACP. A good linear relationship between the  $\Delta F$  and ACP concentration was acquired with the dynamic range of 0.3 to 3 U/L. The regression equation can be fitted as  $\Delta F = 338.6877C_{ACP} + 24.6143$  ( $R^2 = 0.990$ ). The detection limit (LOD) is estimated to be as low as 0.101 U/L according to  $3\sigma$  rule. For colorimetric analysis, as exhibited in Fig. 3D and E, with the raising ACP concentration from 0 U/L to 13 U/L, the absorption peak at 652 nm is continuously dropped down and the color of reaction solution changed from blue to colorless, offering a “turn off” colorimetric signal readout mode for ACP activity. In this regard, the absorbance decreased value  $\Delta A = A_0 - A$  ( $A_0$  and  $A$  are the absorption value of the system at 652 nm without and with ACP, respectively) highly linear correlated to the concentration of ACP from 0.3 U/L to 3 U/L. The regression equation was determined as  $\Delta A = 0.12975C_{ACP} + 0.00763$  with a coefficient of 0.991. The LOD for ACP activity was evaluated to be 0.200 U/L which was calculated by using  $3\sigma$  rule. In comparison with results of previous methods (Table S2), our developed dual-mode fluorescent and colorimetric strategy exhibit comparable analytical performance for ACP activity determination.

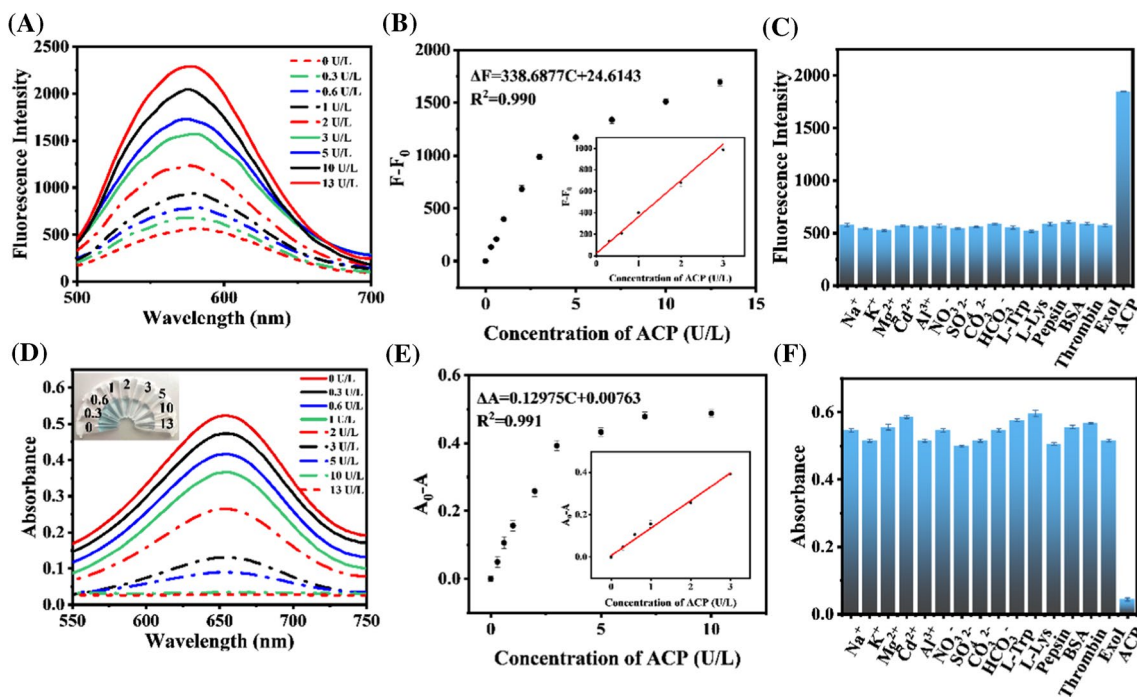


**Fig. 3** Fluorescence spectra (A) and UV–vis spectra (B) for different concentration of ACP. Relationship between fluorescence enhancement (C) and absorbance decrement (D) at different concentration of ACP. Selectivity of fluorescence (E) and colorimetric (F) sensing system

The complexity of real samples presents a challenge for ACP detection not only in sensitivity but also in specificity. Thus, the selectivity of our developed method was evaluated for ACP assay before its practical application. The sensing system was performed with several interferents substance including pepsin, BSA, thrombin, *Exo I*, L-lysine (L-Lys), L-tryptophan (L-Trp),  $K^+$ ,  $Na^+$ ,  $Mg^{2+}$ ,  $Cd^{2+}$ ,  $Al^{3+}$ ,  $NO_3^-$ ,  $SO_4^{2-}$ ,  $CO_3^{2-}$ ,  $HCO_3^-$ . As shown in Fig. 3C and F, the introduction of these interferents can neither cause an obvious fluorescence enhancement nor an apparent absorbance decrement. Therefore, these results suggested that the established dual-mode assay possess good selectivity toward ACP.

Accordingly, to validate the practicability and reliability of the developed dual-mode method for detecting ACP in real sample. The recovery experiments were carried out by spiking ACP standards into blank 10% human serum sample at three concentrations including 0.6, 1.2, 2.4 U/L. As present in Table 1, satisfactory recoveries for the spiked sample

were obtained between 96.66% and 105.83% by using the established dual-mode strategy. These results demonstrated the feasibility and reliability of our proposed method for evaluating the ACP activity in complex samples.

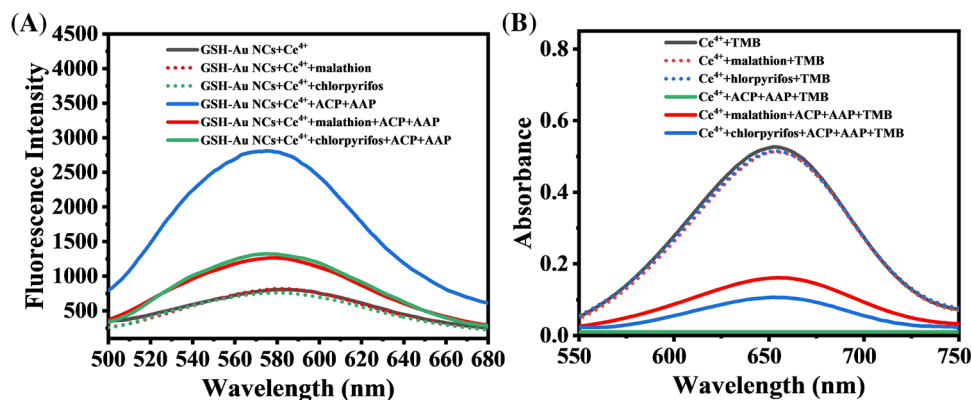
**Potential for screening of ACP inhibitors**

Because of the suppression effect of organophosphorus pesticides (OPs) on ACP, the above strategy was further provided a vital chance for the fabrication of dual-mode platform for screening inhibitor with malathion and chlorpyrifos as representative. To verify the above hypothesis, we firstly investigated the fluorescence response of the GSH-AuNCs +  $Ce^{4+}$  + ACP + AAP system with and without OPs. As verified by Fig. 4A, no significant direct effects of malathion or chlorpyrifos on the fluorescence of GSH-AuNCs +  $Ce^{4+}$  system were observed. However, in comparison with the AuNCs +  $Ce^{4+}$  + ACP + AAP

**Table 1** Detecting of the recovery results for ACP in human sera sample

Mode	Spiked (U/L)	Detected (U/L)	RSD (n=3, %)	Recovery (%)
Fluorescence	0.6	0.62	3.09	103.30
	1.2	1.16	1.90	96.66
	2.4	2.52	3.86	105.00
Colorimetric	0.6	0.63	3.27	105.00
	1.2	1.27	5.56	105.83
	2.4	2.38	4.03	99.17

**Fig. 4** Typical fluorescence spectra (A) and UV-vis spectra (B) in different reaction systems. Reactions were performed in the condition of 10  $\mu\text{g/mL}$  malathion and chlorpyrifos, 0.25 mM AAP, 10 U/L ACP, 40  $\mu\text{M}$   $\text{Ce}^{4+}$ , 5 mM TMB and 5  $\mu\text{L}$  GSH-AuNCs solution



system, when ACP was pretreated with either malathion or chlorpyrifos, the presence of both OPs could suppress the activity of ACP and hinder the fluorescence enhancement. As for the ACP inhibition-based colorimetric assay, the impact of OPs on  $\text{Ce}^{4+}$ -based TMB catalysis is also surveyed. It can be observed from Fig. 4B, the direct interaction between OPs and  $\text{Ce}^{4+}$  can merely influence the oxidase-like activity of  $\text{Ce}^{4+}$ , however, the introduction of OPs into ACP and AAP system can promote the oxidation of TMB. This suggests that OPs effectively inhibit the activity of ACP, resulting in a reduction in the production of AA and impeding the reduction of  $\text{Ce}^{4+}$  to  $\text{Ce}^{3+}$ . Consequently, the AIE was suppressed while the oxidase-like activity of  $\text{Ce}^{4+}$  was restored again.

After concluded by the above discussion, 13 U/L ACP was pretreated with malathion of various concentrations (0.1, 0.25, 0.5, 1, 2, 3, 6, 10, 12  $\mu\text{g/mL}$ ) and chlorpyrifos of different concentrations (0.2, 0.6, 1.5, 2.5, 4, 6, 8, 10, 12  $\mu\text{g/mL}$ ), and then incubated with ACP for additional 15 min to obtain the inhibition curve. As displayed in Fig. 5A-D, the  $\text{IC}_{50}$  values for malathion were determined to be 1.59  $\mu\text{g/mL}$  and 1.52  $\mu\text{g/mL}$  for ACP by using fluorescent and colorimetric method, respectively. And the  $\text{IC}_{50}$  value of chlorpyrifos was calculated to be 2.86  $\mu\text{g/mL}$  for fluorescent assay and 3.00  $\mu\text{g/mL}$  for colorimetric strategy, as revealed by Fig. 5E-H. Also, this dual-mode signal sensing system can offer self-validation and self-correction capability, thus enhancing the reliability of

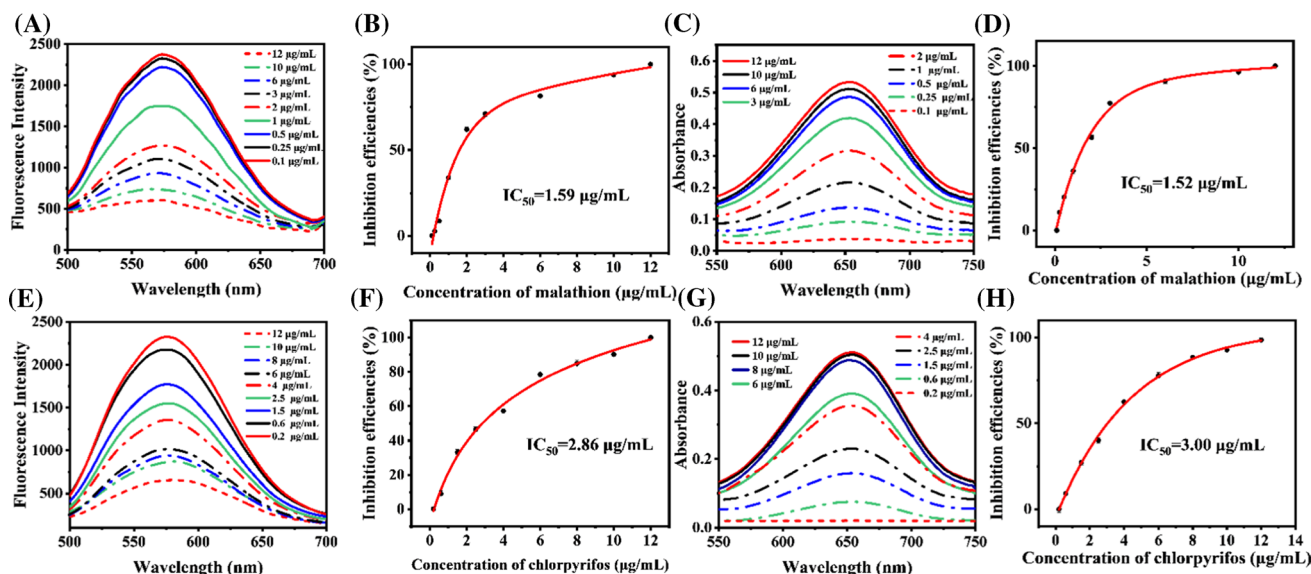


**Fig. 5** Fluorescence spectrum of the sensing system with various concentration of malathion (A) and (B) chlorpyrifos. Standard curve plot of IE in fluorescent assay against the concentration of malathion (C) and (D) chlorpyrifos. UV-vis absorbance spectrum of the sensing

system with various concentration of malathion (E) and (F) chlorpyrifos. Standard curve plot of IE in colorimetric assay against the concentration of malathion (G) and (H) chlorpyrifos



results. Therefore, these evidences confirmed that our sensing method hold the potential for screening of ACP inhibitors.

## Conclusions

In summary, this study presents a simple and dual-mode strategy for quantitative analysis of acid phosphatase activity by cerium ions-directed AIE and oxidase-like activity. The proposed strategy offers several advantages for the study of ACP activity. Firstly, the dual-mode sensing platform enable enhance the reliability and accuracy of ACP activity measurements. Secondly, this strategy exhibits high sensitivity and selectivity towards ACP in biological samples, revealing its excellent practicability. Thirdly, the strategy holds the potential for screening of ACP inhibitors by monitoring the changes in both colorimetric and fluorescence signals. In this contribution, this strategy provides a promising application in rapid, convenient, and accurate detection of ACP activity.

**Supplementary Information** The online version contains supplementary material available at <https://doi.org/10.1007/s00216-023-05103-w>.

**Acknowledgements** This work was supported by the National Natural Science Foundation of China (21705042), Natural Science Foundation of Hunan Province (2021JJ40169), the Scientific Research Foundation of Hunan Provincial Education Department (22B0608).

## References

- Vernon CA, Gauldie J, Hanson JM, Humphreys JM, Smith PE, Lawrence AJ, Banks BEC. Acid phosphatases. *Nature*. 1965;208:382–3.
- Deng SR, Lu LH, Li JY, Du ZZ, Liu TT, Li WJ, Xu FS, Shi L, Shou HX, Wang C. Purple acid phosphatase 10c encodes a major acid phosphatase and regulates the plant growth under phosphate deficient condition in rice. *J Exp Bot*. 2020;71(14):4321–32.
- Bottini E, Carapella E, Scacchi R, Lucarini N, Gloria-Bottini F, Pascone R, Bonci E, Maggioni G. Serum haptoglobin appearance during neonatal period is associated with acid phosphatase (ACP1) phenotype. *Early Human Dev*. 1985;10(3–4):237–43.
- Howard PJ, Fraley EE. Elevation of the acid phosphatase in benign prostatic disease. *J Urol*. 1965;94(6):687–90.
- Han YX, Quan KJ, Chen J, Qiu HD. Advances and prospects on acid phosphatase biosensor. *Biosens Bioelectron*. 2020;170:112671.
- Dai MS, Lo HC, Chen LJ, Tseng SF. Prognostic significance of tartrate-resistant acid phosphatase expression in breast cancer. *J Clin Oncol*. 2019;37(15):12594–5.
- Yamauchi YJ, Ido M, Ohta M, Maeda H. High performance liquid chromatography with an electrochemical detector in the cathodic mode as a tool for the determination of p-nitrophenol and assay of acid phosphatase in urine samples. *Chem Pharm Bull*. 2004;52(5):552–5.
- Huang MJ, Tian JY, Zhou CH, Bai P, Lu JS. Photoelectrochemical determination for acid phosphatase activity based on an electron inhibition strategy. *Sens Actuators, B Chem*. 2020;307:127654.
- Foti AG, Herschman H, Cooper JF. Comparison of human prostatic acid phosphatase by measurement of enzymatic activity and by radioimmuno-assay. *Clin Chem*. 1977;23(1):95–9.
- Na WD, Hu TY, Su XG. Sensitive detection of acid phosphatase based on graphene quantum dots nanoassembly. *Analyst*. 2016;16(141):4926–32.
- Chena YY, Wanga ZZ, Hao XL, Li FL, Zheng YJ, Zhang JZ, Lin XH, Weng SH. Selective and sensitive fluorescent monitoring of acid phosphatase (ACP) activity under neutral conditions through the ACP enzymatic catalysis of dopamine as a new substrate to polydopamine. *Sens Actuators, B Chem*. 2019;297:12678.
- Al-mashriqi HS, Zheng HH, Qi SD, Zhai HL. Gold nanoclusters reversible switches based on aluminum ions-triggered for detection of pyrophosphate and acid phosphatase activity. *J Mol Struct*. 2021;1242:130755.
- Zhu ZM, Lin XY, Wu LN, Zhao CF, Li SG, Liu AL, Lin XH, Lin LQ. Nitrogen-doped carbon dots as a ratiometric fluorescent probe for determination of the activity of acid phosphatase, for inhibitor screening, and for intracellular imaging. *Microchim Acta*. 2019;186:558.
- Qian ZS, Chai LJ, Zhou Q, Huang YY, Tang C, Chen JR, Feng H. Reversible fluorescent nanoswitch based on carbon quantum dots nanoassembly for real-time acid phosphatase activity monitoring. *Anal Chem*. 2015;87(14):7332–9.
- Zheng SS, Gu HZ, Yin DY, Zhang JL, Li W, Fu Y. Biogenic synthesis of AuPd nanocluster as a peroxidase mimic and its application for colorimetric assay of acid phosphatase. *Colloids Surf, A*. 2020;589(20):124444.
- Liu P, Zhao MG, Zhu HJ, Zhang ML, Li X, Wang MZ, Liu BX, Pan JM, Ni XH. Dual-mode fluorescence and colorimetric detection of pesticides realized by integrating stimulus-responsive luminescence with oxidase-mimetic activity into cerium-based coordination polymer nanoparticles. *J Hazard Mater*. 2022;423:127077.
- Li Q, Guo YM, He XY, Li GL. Bifunctional Cu(II)-containing PDA-PEI copolymer dots: demonstration of a dual-mode platform for colorimetric-fluorescent detection of glyphosate in the environment. *Talanta*. 2023;265(1):124865.
- Xia M, Zhao XE, Sun J, Zheng ZJ, Zhu SY. Graphene quantum dots combined with the oxidase-mimicking activity of Ce<sup>4+</sup> for ratiometric fluorescent detection of Ce<sup>4+</sup> and alendronate sodium. *Sens Actuators, B Chem*. 2020;319(15):128321.
- Liang L, Zhao ZH, Ye FG, Zhao SL. Rapid and sensitive colorimetric detection of dopamine based on the enhanced-oxidase mimicking activity of cerium(IV). *New J Chem*. 2021;45:6780–6.
- Pu S, Shi CT, Zhang JL, Hou XD, Wu L. Ce<sup>4+</sup>-based self-validated portable platform for highly selective and anti-interference visual sensing of phosphate. *Sens Actuators, B Chem*. 2023;393(15):134245.
- Li Q, Guo YM, He XY, Li GL. Sensitive and label-free colorimetric detection of glyphosate based on the suppression peroxidase-mimicking activity of Cu(II) ions. *Molecules*. 2023;28(12):4630.
- Song HW, Wang HY, Li X, Peng YX, Pan JM, Niu XH. Sensitive and selective colorimetric detection of alkaline phosphatase activity based on phosphate anion-quenched oxidase-mimicking activity of Ce(IV) ions. *Anal Chim Acta*. 2018;1044(31):154–61.
- Peng HP, Jian ML, Huang ZN, Wang WJ, Deng HH, Wu WH, Liu AL, Xia XH, Chen W. Facile electrochemiluminescence sensing platform based on high-quantum-yield gold nanocluster probe for ultrasensitive glutathione detection. *Biosens Bioelectron*. 2018;105(15):71–6.
- Qi DY, Wang C, Gao YC, Li HW, Wu YQ. Heteroatom doping and supramolecular assembly promoted copper nanoclusters to be a stable & high fluorescence sensor for trace

- amounts of ATP determination. *Sens Actuators, B Chem.* 2022;358:131469.
25. Wu YF, Gao YF, Du JX. Bifunctional gold nanoclusters enable ratiometric fluorescence nanosensing of hydrogen peroxide and glucose. *Talanta.* 2019;197(15):599–604.
  26. Liu YB, Zhang Y, Zhang W, Wang XH, Sun Y, Huang YB, Ma PY, Ding J, Song DQ. Ratiometric fluorescent sensor based on MoS<sub>2</sub> QDs and AuNCs for determination and bioimaging of alkaline phosphatase. *Spectrochim Acta Part A Mol Biomol Spectrosc.* 2021;262(5):120087.
  27. Luo ZT, Yuan X, Yu Y, Zhang QB, Leong DT, Lee JY, Xie JP. From aggregation-induced emission of Au(I)-thiolate complexes to ultrabright Au(0)@Au(I)-thiolate core-shell nanoclusters. *J Am Chem Soc.* 2012;134(40):16662–70.
  28. Kateshiya MR, Malek NI, Murthy ZVP, Kailasa SK. Designing of glutathionelactose derivative for the fabrication of gold nanoclusters with red fluorescence: sensing of Al<sup>3+</sup> and Cu<sup>2+</sup> ions with two different mechanisms. *Opt Mater.* 2020;100:109704.
  29. Qu F, Zhao LY, Han WL, You JM. Ratiometric detection of Zn<sup>2+</sup> and Cd<sup>2+</sup> based on self-assembled nanoarchitectures with dual emissions involving aggregation enhanced emission (AEE) and its application. *J Mater Chem B.* 2018;6(30):4995–5002.
  30. Wu XT, Li CX, Liao SC, Li L, Wang TT, Su ZM, Wang CG, Zhao JH, Sui CP, Lin J. Silica encapsulated Gd<sup>3+</sup>-aggregated gold nanoclusters for in vitro and in vivo multimodal cancer imaging. *Chem Eur J.* 2014;20(29):8876–82.
  31. Ji LY, Guo YH, Hong SN, Wang ZL, Wang KW, Chen X, Zhang JY, Hu JM, Pei RJ. Label-free detection of Pb<sup>2+</sup> based on aggregation-induced emission enhancement of Au-nanoclusters. *RSC Adv.* 2015;5(46):36582–6.

**Publisher's Note** Springer Nature remains neutral with regard to jurisdictional claims in published maps and institutional affiliations.

Springer Nature or its licensor (e.g. a society or other partner) holds exclusive rights to this article under a publishing agreement with the author(s) or other rightsholder(s); author self-archiving of the accepted manuscript version of this article is solely governed by the terms of such publishing agreement and applicable law.